Inorganic Chemistry

Article

pubs.acs.org/IC

$CaSO_4$ and Its Pressure-Induced Phase Transitions. A Density Functional Theory Study

Lourdes Gracia,*[,†,‡] Armando Beltrán,[†,‡] Daniel Errandonea,[‡,§] and Juan Andrés[†,‡]

[†]Departament Química Física i Analítica, Universitat Jaume I, 12071 Castelló de la Plana, Spain

[§]Departamento de Física Aplicada-ICMUV, Universidad de Valencia, Edificio de Investigación, C/Dr. Moliner 50, 46100 Burjassot, Valencia, Spain

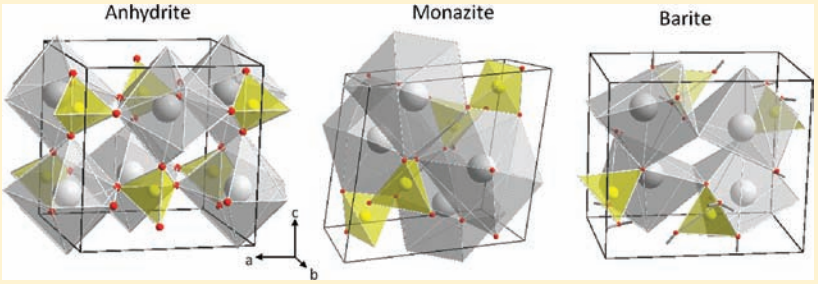

ABSTRACT: Theoretical investigations concerning possible calcium sulfate, $CaSO_4$, high-pressure polymorphs have been carried out. Total-energy calculations and geometry optimizations have been performed by using density functional theory at the B3LYP level for all crystal structures considered. The following sequence of pressure-driven structural transitions has been found: anhydrite, *Cmcm* (in parentheses the transition pressure) → monazite-type, $P2_1/n$ (5 GPa) → barite-type, *Pnma* (8 GPa), and scheelite-type, $I4_1/a$ (8 GPa). The equation of state of the different polymorphs is determined, while their corresponding vibrational properties have been calculated and compared with previous theoretical results and experimental data.

1. INTRODUCTION

Anhydrite, anhydrous calcium sulfate ($CaSO_4$), is perhaps the prototypical simple sulfate salt and one of the most important rock-forming minerals. It has an orthorhombic structure with space group *Cmcm* formed from dehydration of gypsum ($CaSO_4{\cdot}2H_2O$). It is known to absorb water from the environment to be converted into hydrates like gypsum and bassanite ($2CaSO_4{\cdot}H_2O$). The structure adopted by anhydrite is not shared by any other compounds belonging to the $A^{2+}B^{6+}O_4$ family. In particular, it is not isomorphous with orthorhombic barium (barite), $BaSO_4$, and strontium (celestine), $SrSO_4$, sulfates, as might be expected from the chemical formulas. However, the crystal structure of anhydrite, consisting of CaO_8 bisdisphenoids and nearly ideal SO_4 tetrahedra (see Figure 1), has many similarities with those of important ABO_4 oxides like zircon ($ZrSiO_4$) and scheelite ($CaWO_4$).[1] In the last years, the pressure-induced polymorphism of ABO_4 compounds has attracted considerable attention. In particular, several pressure-induced phase transitions have been discovered.[2−4] According with crystal-chemistry arguments, as a first approximation, the high-pressure structural sequences of ABO_4 oxides can be understood by comparing the size of their constitutent atoms. In particular, compounds with small-size cations may take under compression the structure of compounds with large-size cations. In the case of alkaline-earth sulfates, the large-cation sulfates crystallize in nature in the barite structure and the small-cation sulfate in the anhydrite and $CrVO_4$ structures.[5] Thus, following the example of the carbonates and silver perchlorate, one would expect that $CaSO_4$ should adopt the barite structure at high pressures.

Evidence of a pressure-induced phase transition in anhydrite was first found in shocked $CaSO_4$ after the 1964 Salmon nuclear test.[6] More recently, different diamond-anvil-cell experiments found high-pressure polymorphs for $CaSO_4$. A study using X-ray diffraction techniques and Raman spectroscopy reported that anhydrite at 21 GPa after laser irradiation transformed to a high-pressure modification with an orthorhombic cell.[7] However, an anhydrite-to-monazite phase transition was previously proposed by Borg and Smith.[8] Later studies confirmed the existence of the monazite-type ($CePO_4$) structure as a postanhydrite phase at 11.8 GPa[9] and reported additional transformations to the barite- (at 21.4 GPa and 1450 K) and $AgMnO_4$-type structure (upon decompression from barite at 19.9 GPa and 295 K). The monazite-to-barite transformation was also encountered in $LaPO_4$ at high pressures and room temperature but at higher pressure than that in $CaSO_4$.[10] Observation of the barite variant, and its distorted $AgMnO_4$ precursor, was already predicted by Pistorius et al.[11] as a postanhydrite phase. However, more recent works[12,13] based on X-ray diffraction and Raman scattering on $CaSO_4$ found apparently contradictory conclusions. The phase transformation to the monazite type under cold compression was found at much lower pressure, 2−5 GPa instead of 11.8

Received: September 21, 2011
Published: December 19, 2011

 © 2011 American Chemical Society dx.doi.org/10.1021/ic202056b | *Inorg. Chem.* 2012, 51, 1751−1759

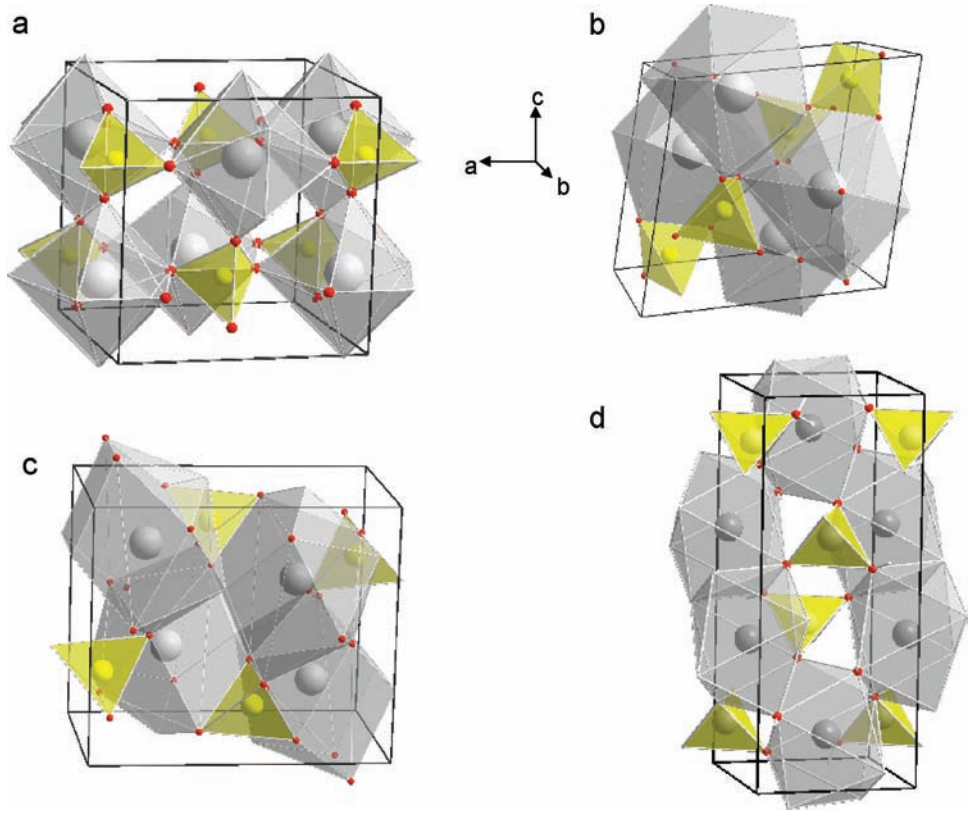

Figure 1. Structures of $CaSO_4$: (a) anhydrite; (b) monazite; (c) barite; (d) scheelite.

GPa. In addition, the monazite phase was found to be stable up to nearly 30 GPa, with another phase transition being found at 33 GPa and 1800 K. This phase is not compatible with the barite, $AgMnO_4$, or scheelite forms.[12]

The above-described facts indicate that additional work is requested to fully understand the sequence of the postanhydrite phases in $CaSO_4$. In this respect, first-principles calculations[14] can become a powerful complement to experimental techniques, to provide detailed structural information and to understand, at the atomic level, phenomena such as polymorphism and pressure-induced transformations. In this work, we performed such calculations. Besides monazite and barite structures, we have explored other potential postanhydrite candidates such as scheelite (adopted by $CaSeO_4$), orthorhombic structure $P2_12_12_1$ (shown in $CaSeO_4$ and $BaSO_4$[15]), and $AgMnO_4$[9] (not previously encountered in group II−VI oxides). In addition to contributing to the understanding of the high-pressure behavior of $CaSO_4$, the reported results can be of importance in establishing a bridge between "lower-pressure" smaller-cation sulfates and chromates, anticipated "moderate-pressure" large cation forms of sulfates and chromates that crystallize in monazite- and barite-type structures, and the "high-pressure" structures of the selenates, molybdates, and tungstates that form in primarily barite- and scheelite-type structures.[16] Recently, Clavier et al.[17] have reviewed the ABO_4 monazite-type compounds from an extended family in terms of field of stability versus composition. The phosphate, vanadate, chromate, arsenate, sulfate, and silicate families are described, and the stability limits of the monazite-type structure are discussed versus several models generally correlated with geometric criteria. Therefore, our results can also be important for many ABO_4 oxides.

The aim of this work is to improve the understanding of the behavior of $CaSO_4$ under compression. As an alternative to experimental techniques, we will investigate the structural and vibrational properties of $CaSO_4$ under high pressure up to 25 GPa in the frame of density functional theory (DFT) by the nonlocal B3LYP approximation. The paper is organized as follows: Section 2 details the computational strategy. In section 3, we present our theoretical results together with the discussion concerning the structural properties, phase stability, and vibrational analysis. Finally, we summarize our main conclusions in section 4.

2. COMPUTATIONAL DETAILS

In this study, calculations were performed with the *CRYSTAL09* program package.[18] S and Ca atoms have been described by 86-311G* and 86-511d21G basis sets, respectively, while for O atoms, the standard 6-31G* basis set has been used. Becke's three-parameter hybrid nonlocal exchange functional,[19] combined with the Lee−Yang−Parr gradient-corrected correlation functional, B3LYP,[20] has been used. This functional has been extensively used for molecules and crystalline structures, providing an accurate description of the bond lengths, phonons, binding energies, and band-gap values.[21−23] Diagonalization of the Fock matrix was performed at adequate *k*-point grids in reciprocal space, with the Pack−Monkhorst/Gilat shrinking factors being IS = ISP = 4 (21, 30, 27, and 14 *k* points for anhydrite, monazite, barite, and scheelite, respectively). The thresholds controlling the accuracy of the calculation of Coulomb and exchange integrals were set to 10^{-8} (ITOL1 to ITOL4) and 10^{-14} (ITOL5), whereas the percent of Fock/Kohn−Sham matrix mixing was set to 40.[18] Fittings with a Birch−Murnaghan third- and second-order equation of state (EOS) of the computed energy−volume data provide values of the zero-pressure bulk modulus (B_0) and its pressure derivative (B_0') as well as enthalpy−pressure curves for the polymorphs studied.[24] Vibrational-frequency calculations in *CRYSTAL* are performed at the Γ point within the harmonic approximation, and

dx.doi.org/10.1021/ic202056b | *Inorg. Chem.* 2012, 51, 1751−1759

the dynamical matrix is computed. Nevertheless, the Hessian matrix is even more sensible on the precision and calculation levels of electronic energy calculation by numerical evaluation of the first derivative of the analytical atomic gradients.

3. RESULTS AND DISCUSSION

3.1. Structural Properties. In order to identify high-pressure phase transitions, we carried out first-principles calculations of the initial anhydrite structure and five potential different phases at high pressure: monazite-type ($P2_1/n$), barite-type ($Pnma$), scheelite-type ($I4_1/a$), $AgMnO_4$-type ($P2_1/n$), and orthorhombic $CaSeO_4$-type ($P2_12_12_1$) structures. The structural candidates considered were selected by empirical crystallochemical arguments such as Bastide's diagram[2] and the behavior under pressure of the cation subarrays in oxides. Thus, the monazite-, barite-, and scheelite-type structures could be high-pressure phases in $CaSO_4$ because they occur, for example, in other ABO_4 compounds like $TbPO_4$ or YPO_4.[25,26] Other possible high-pressure phases are the $AgMnO_4$-type structure, which is a monoclinic distortion of the barite-type structure, observed in $CaSO_4$ under decompression from the barite structure,[9] or the orthorhombic $CaSeO_4$ phase ($P2_12_12_1$), which has been observed in a recent study of barite $BaSO_4$.[15]

In the anhydrite structure (Figure 1a), Ca atoms are in 8-fold coordination with O atoms, but the coordination polyhedron is not the normal cube. Instead, it has 12 triangular faces, with the shape of a snub disphenoid (two pentagonal pyramids joined base to base but with two edges not attached). The main structural features of the anhydrite were reported by Kirfel and Will.[27] Each S atom is coordinated by four O atoms (1.547 Å), forming an almost regular SO_4 tetrahedron, while each Ca atom is coordinated by eight O atoms with four Ca−O distances (2.367, 2.490, 2.500, and 2.559 Å), forming a dodecahedron considerably distorted with strongly contracted edges shared with the SO_4 groups.

The monazite phase is a monoclinic structure, which belongs to the space group $P2_1/n$. The cell contains four formula units for a total of 24 atoms. In the cell (see Figure 1b), all of the atoms reside in the 4e (x, y, z) sites according to the Wyckoff notation. Ca or S atoms take only one crystallographic equivalent site, and they are 9- and 4-fold-coordinated to O atoms, respectively.

The barite structure consists of triangular prisms of Ca atoms that share faces along the b direction and corners in the other two directions, with the [SO_4] groups inserted into these metal prisms (see Figure 1c).[28] In the barite structure each [CaO_{12}] polyhedron shares three edges and five triangular faces with the adjacent [CaO_{12}].

From the cationic point of view, the scheelite structure consists of two intercalated diamond lattices: one for A cations and another for B cations. The Ca atoms are coordinated by eight O anions with two different distances, thus forming CaO_8 polyhedral units. On the other hand, S atoms are coordinated by four O anions, forming relatively isolated SO_4 tetrahedral units. The CaO_8 dodecahedra in scheelite share edges with adjacent CaO_8 polyhedra, forming zigzag chains along the c axis. These chains are cross-linked through SO_4 tetrahedra by sharing corners with them (see Figure 1d). Actually, anhydrite and scheelite are related structures containing bisdisphenoids.[1] In scheelite, the Ca atoms are enclosed by eight O atoms at the corners of a *square antiprism*; in anhydrite, the disphenoid is created by separating opposing pairs of tetrahedral faces and joining their vertices with a zigzag belt of equilateral triangles.

The orthorhombic $CaSeO_4$ phase ($P2_12_12_1$) and the monoclinic $AgMnO_4$ type as high-pressure postbarite candidates have also been studied. The first structure has been observed in a recent study of barite $BaSO_4$.[15] It is basically a strong distortion of the barite phase, where the a axis contracts and the b axis expands without introducing large changes in the unit-cell volume. The $AgMnO_4$-type structure has been observed in $CaSO_4$.[9] It is also a distortion of barite that consists of stacks of SO_4 tetrahedra and rows of Ca atoms extending in the c direction.[29] In both structures, the B cation is tetrahedrally coordinated and the A cation is 12-coordinated by O atoms.

Structural data of the phases that we found could become stable upon compression are collected in Table 1. For comparison, structures experimentally found at different $P-T$ conditions are shown in Table 2. Our theoretical study indicates that anhydrite is the structure of $CaSO_4$ with the lowest enthalpy at ambient pressure. The equilibrium volume V_0 is overestimated by ~4.8% with respect to the experimental value.[12] This difference is typical of DFT calculations at the B3LYP level.[30,31] Full structural information of the anhydrite structure shows a good agreement between theory and

Table 1. Structural Parameters and Bulk Properties for the $CaSO_4$ Polymorphs[a]

	site	x	y	z
Anhydrite $Cmcm$: a = 7.1051 Å, b = 6.3048 Å, c = 7.1434 Å, B_0 = 63.9 GPa, B_0' = 5.9				
Ca	4c	0	0.6516	0.25
S	4c	0	0.1547	0.25
O	8g	0.1739	0.0071	0.25
O	8f	0	0.3056	0.0792
Monazite $P2_1/n$: a = 6.7528 Å, b = 6.9816 Å, c = 6.4318 Å, β = 103.38, B_0 = 146.0 GPa, B_0' = 4				
Ca	4e	0.2815	0.1593	0.1001
S	4e	0.3048	0.1630	0.6121
O	4e	0.2501	0.0068	0.4450
O	4e	0.3814	0.3307	0.4975
O	4e	0.4742	0.1070	0.8037
O	4e	0.1274	0.2153	0.7104
Barite $Pnma$: a = 7.8437 Å, b = 5.1947 Å, c = 6.7493 Å, B_0 = 160.4 GPa, B_0' = 4				
Ca	4c	0.1896	0.25	0.1798
S	4c	0.4434	0.25	0.1817
O	4c	0.6148	0.25	0.0760
O	4c	0.2899	0.25	0.0401
O	8d	0.4320	0.9928	0.3138
Scheelite $I4_1/a$: a = 4.8434 Å, c = 11.5096 Å, B_0 = 163.4 GPa, B_0' = 4				
Ca	4b	0	0.25	0.625
S	4a	0	0.25	0.125
O	16f	0.2406	0.1348	0.0518
$P2_12_12_1$: a = 6.7849 Å, b = 5.5814 Å, c = 6.0885 Å				
Ca	4a	0.6421	0.2842	0.5745
S	4a	0.5967	0.2446	0.0769
O	4a	0.4343	0.1952	0.2399
O	4a	0.7740	0.3256	0.2053
O	4a	0.4578	0.9394	0.5833
O	4a	0.6441	0.0210	0.9399

[a]Anhydrite at 10^{-4} GPa (atmospheric pressure), monazite at 4.92 GPa, barite at 6.96 GPa, scheelite at 7.11 GPa, and orthorhombic $P2_12_12_1$ at 32.0 GPa. For the last phase, the bulk modulus is not reported because it cannot be accurately calculated within the pressure range of this study (the phase becomes stable beyond 30 GPa).

dx.doi.org/10.1021/ic202056b | Inorg. Chem. 2012, 51, 1751−1759

Table 2. Structural Parameters for the $CaSO_4$ Polymorphs from Bibliography

	site	x	y	z
Anhydrite:[12] a = 6.992 Å, b = 6.240 Å, c = 6.999 Å				
Anhydrite:[27] a = 6.998 Å, b = 6.245 Å, c = 7.006 Å				
Ca	4c	0	0.6524	0.25
S	4c	0	0.1556	0.25
O	8g	0.1695	0.0155	0.25
O	8f	0	0.2976	0.0817
Monazite:[9] a = 6.377 Å, b = 6.644 Å, c = 6.167 Å, and β = 102.22 at 11.8 GPa				
Ca	4e	0.2685	0.1592	0.0981
S	4e	0.3036	0.1664	0.6278
O	4e	0.2488	0.0003	0.4401
O	4e	0.3573	0.3480	0.4915
O	4e	0.4745	0.1197	0.7932
O	4e	0.1192	0.2202	0.7110
Monazite:[12] a = 6.829 Å, b = 7.134 Å, c = 6.228 Å, and β = 104.39 at 10.5 GPa				
Monazite:[13] a = 6.35 Å, b = 6.74 Å, c = 6.13 Å, and β = 103.9 at 7.8 GPa				
Barite:[9] a = 6.3365 Å, b = 4.9532 Å, and c = 7.5347 Å at 21 GPa				
Ca	4c	0.1812	0.25	0.1696
S	4c	0.5606	0.25	0.8166
O	4c	0.8898	0.25	0.5675
O	4c	0.2141	0.25	0.5341
O	8d	0.4287	0.9823	0.3193

experiment. In particular, the agreement is quite good regarding atomic positions.

Figure 2 shows the energy versus volume curves for the ambient and high-pressure structures. As shown in the enthalpy

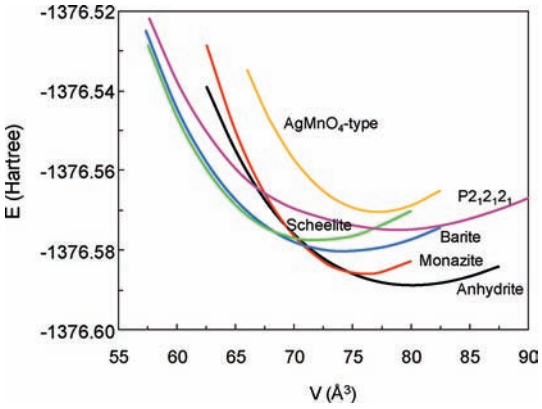

Figure 2. Internal energy (hartrees) versus volume (Å^3) per formula unit for the $CaSO_4$ polymorphs.

as a function of pressure curves of Figure 3a, the monazite phase becomes more stable than anhydrite at 5 GPa, after a transition in which the volume change is about 1.7%. This transition is found at an intermediate pressure compared to previous experiments of 11.8[9] and 2 GPa[12] and compares very well with the anhydrite–monazite coexistence found up to 5 GPa by Bradbury and Williams.[13] For the low-pressure anhydrite phase, we obtain a bulk modulus value of 63.9 GPa. The value of B_0' is ~6. Experimentally, Stephens[32] determined a B_0 value near 45 GPa and found a very sluggish phase transition in the range 1.96–3.40 GPa, with a volume change of 4.1%. Our theoretical volume and B_0 are overestimated for anhydrite. However, the differences in the bulk modulus can be caused by the fact that experiments were

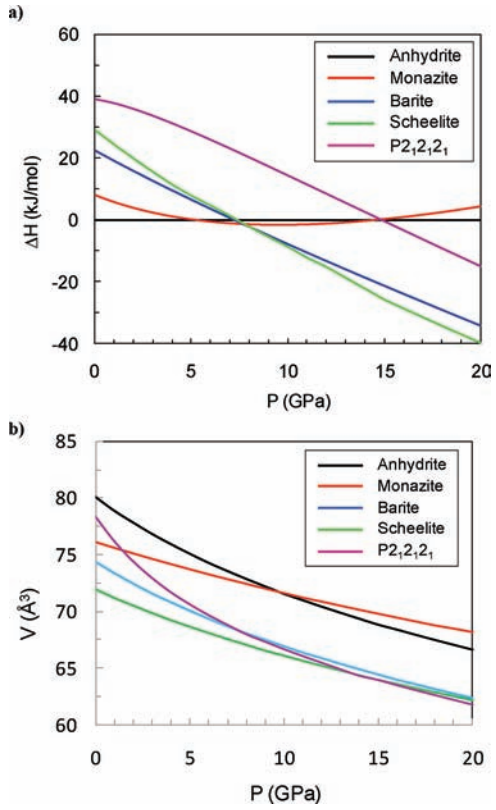

Figure 3. (a) Enthalpy versus pressure curve for the $CaSO_4$ polymorphs, taking the anhydrite structure as the reference. (b) Volume per formula unit versus pressure curve for the $CaSO_4$ polymorphs.

carried out under nonuniform stress, with the pressure not being measured in situ.

Anhydrite–monazite structural relationships were recently reviewed,[17] suggesting that the anhydrite-to-monazite transition is mostly displacive in nature. This is due to the alternative rotation (±45°) of the tetrahedral orientation about the axis of the chains formed by CaO_8 and SO_4 polyhedra linked by shared edges. To preserve the chains, the two structures are related through axial transformation. Apparently, compression of the monazite phase is isotropic. We found also that the β angle is basically not affected by compression. It also involves a change of the Ca coordination from 8 to 9, but the S coordination remains 4. The displacive character of the transition is coherent with a large difference in transition pressures experimentally observed.[9,12,32] In these kinds of transitions, different pressure environments (e.g., changes in hydrostaticity) may strongly affect the transition pressure.[33,34] For the monoclinic phase, we determined the EOS with B_0 = 146 GPa and B_0' = 4, which agrees very well with the experimental value reported by Bradbury and Williams[13] of 151.2 GPa, a bulk modulus approximately 3 times as large as that of anhydrite. This decrease of the bulk compressibility is caused by the rearrangement of the polyhedral units that takes place at the transition. Regarding the polyhedral changes taking place at the phase transition, calculations show that distortion of the SO_4 tetrahedra is enhanced in the monoclinic phase and that the Ca–O bonds are strongly enlarged at the orthorhombic-to-monoclinic transition. The average Ca–O bond distances are increased by 5.1% at the transition.

dx.doi.org/10.1021/ic202056b | Inorg. Chem. 2012, 51, 1751–1759

Upon further compression, we found that according to calculations the barite- and scheelite-type structures become thermodynamically more stable than monazite and anhydrite. Both phases are very competitive with very similar enthalpy. Monazite becomes energetically less favored than these structures at 8 GPa. The monazite-to-barite transformation is reported to occur at 21.4 GPa after heating of the $CaSO_4$ high-pressure monazite form at T = 1450 K.[9,16] At room temperature, the transition was not experimentally found. This suggests the existence of a large kinetic barrier preventing the occurrence of the transition. The existence of a kinetic barrier seems to be a reasonable proposition because the monazite-to-barite transition involves an important atomic rearrangement. In particular, the transition implies an increase of the coordination of the Ca cation from 9 in monazite to 12 in barite, without almost no changes in the SO_4 tetrahedra. The average Ca−O bond distances are increased by 6.3% at the transition pressure of 8 GPa. On the other hand, also nonhydrostaticity could influence the experimental studies because experiments were performed under nonhydrostatic conditions. These conditions are known to influence the structural sequences of ABO_4 oxides,[35] and therefore experiments using neon or helium as a pressure-transmitting medium are needed to discard this hypothesis.

According to our calculations, the monazite-to-scheelite transformation occurs at the same pressure as the monazite-to-barite transition (8 GPa). This transition takes place also for $CeVO_4$,[36] $PrAsO_4$, $NdAsO_4$,[37] and $BiAsO_4$.[17,38] Macey[39] describes the monazite-to-scheelite transformation by sharing the parallel planes to (001) and (010) of monazite, to become the closest packed cation planes in the scheelite form. In this case, atomic movements within the planes are also necessary to reach the scheelite packing, with a reconstructive transformation. The transition to scheelite involves a larger volume collapse than the transition to barite (see Figure 3b). It also requires a more important reconstruction of the crystalline structure. Therefore, one could expect larger kinetic barriers for the monazite-to-scheelite transition than for the monazite-to-barite transition. This fact could be the cause for observation of the second transition under high-pressure and high-temperature conditions.[9] It is important to note here that, as expected, we found the high-pressure barite- and scheelite-type phases to be less compressible than the phases found at lower pressure (their bulk modulus is close to 160 GPa; see Table 1).

Calculations up to 25 GPa do not find evidence of additional phase transition. However, extrapolation of our results to higher pressure suggests that beyond 25 GPa the orthorhombic $P2_12_12_1$ structure could become thermodynamically the most stable phase pointing toward the occurrence of a third pressure-driven transition. This orthorhombic structure is basically a strong distortion of the barite phase, where the a axis contracts approximately 10.7%, the b axis expands approximately 13.1%, and the c axis remains nearly constant up to 30 GPa (a pressure above which the possible transition is predicted), with the volume of both phases differing by only ∼0.5%. This lattice transformation entails a small displacement and tilting movement of the $[SO_4]$ tetrahedra, and the elongation of the b axis implies the nonexistence of trigonal prisms. This phase could be compatible with the structure found by Ma et al.[12] at 1800 K stable up to 33 GPa.

Changes in the crystal structures induced by the phase transitions can also be related to different local atomic rearrangements in the crystals. Thus, the higher density of the high-pressure structures can be traced back to the unit-cell volume reduction due to a more effective packing of the O atoms surrounding the Ca atoms. To analyze pressure effects from this perspective, we calculated the pressure evolution of the Ca−O and S−O bond distances for the four reported phases, and the results are depicted in Figure 4. Calculations are

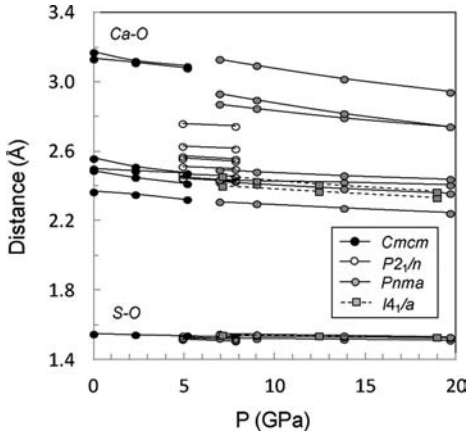

Figure 4. Pressure evolution of Ca−O and S−O distances for the different phases of $CaSO_4$.

capable of accurately describing the evolution and changes induced by the pressure in atomic bonds. Four, eight, seven, and two different Ca−O distances are found for anhydrite, monazite, barite, and scheelite, respectively. At the same time, two, four, three, and one different S−O distances are found for anhydrite, monazite, barite, and scheelite, respectively. An analysis of Figure 4 points out that in the four phases the Ca−O bonds are more compressible than the S−O bonds; i.e., the SO_4 tetrahedra behave like rigid units. The difference on the bond compressibility is more notorious in the low-pressure tetragonal phase. Another fact to remark is that at the second phase transition, from monazite to barite, the induced coordination change produces an enlargement of the Ca−O bonds in order to accommodate three new O atoms surrounding the Ca atoms. Therefore, the coordination of the S atom almost does not change along with pressure and is maintained at 4. However, the tilting movement of the $[SO_4]$ tetrahedra led to a change in the environment of the Ca atoms and to the phase transition. Consequently, a progressive change in the coordinates of most of the atoms gives rise to an increase of the Ca coordination number from 8 in anhydrite to 9 in monazite and 12 in barite at 5 and 8 GPa, respectively. This agrees with the system proposed by Bastide and extended by Errandonea and Manjon.[2] On the other hand, the change and distortion of Ca−O polyhedra and the behavior of SO_4 tetrahedra as nearly incompressible units are consistent with the fact that Ca−O bonds are weaker than S−O bonds.

To close this section, we present the pressure evolution of the unit-cell parameters of $CaSO_4$. Their pressure dependence is plotted in Figure 5. There it can be seen that compression of anhydrite and scheelite is highly anisotropic, with κ_c (0.0245 GPa^{-1}) > κ_a (0.0218 GPa^{-1}) > κ_b (0.0148 GPa^{-1}) for the anhydrite phase and κ_c (0.0378 GPa^{-1}) > κ_a (0.0099 GPa^{-1}) for the scheelite phase, compared to the monazite and barite phases, whose lattice parameter contraction is rather isotropic. The large compressibility of the c axis is due to the fact that the CaO_8 polyhedral chains are aligned along this axis, whereas

dx.doi.org/10.1021/ic202056b | Inorg. Chem. 2012, 51, 1751−1759

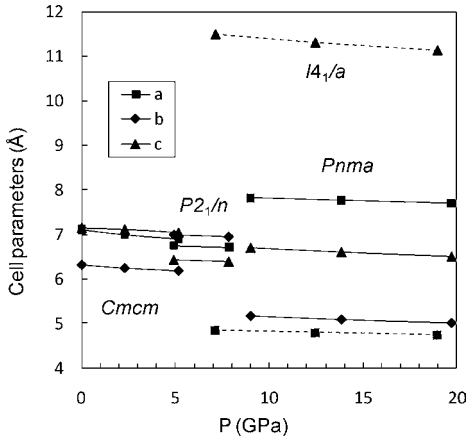

Figure 5. Pressure evolution of the unit-cell parameters of $CaSO_4$.

along the other directions, SO_4 and CaO_8 units are intercalated. Therefore, because pressure produces basically a reduction of the Ca−O bonds, the *c* axis should be the most compressible axes in the anhydrite and scheelite phases. Bradbury and Williams[13] pointed out that compression in the monazite structure occurred dominantly in the *a* and *b* directions, with the *c* parameter and β angle being nearly unchanged with pressure. This behavior seems to be typical of experiments under nonhydrostatic conditions. However, our results show an isotropic contraction of all parameters. The quasi-isotropic compression agrees with the behavior observed in monazite-type phosphates when compressed under nearly hydrostatic conditions using neon as the pressure-transmitting medium.[10]

3.2. Vibrational Analysis. Lattice vibrations play an important role for materials modeling, and their behavior under pressure provides useful information regarding structural instabilities and phase transformation. The frequencies of Raman-active modes for the anhydrite, monazite, barite, and scheelite structures have been calculated as well as their pressure dependences.

According to group-theory analysis, anhydrite displays 18 Raman-active modes corresponding to the following decomposition at the Γ point:

$$\Gamma = 6A_g + 5B_{1g} + 5B_{2g} + 2B_{3g}$$

In Table 3, the symmetry and assignment of Raman-active modes for anhydrite are presented, compared to the experimental values. The internal modes of the SO_4 units are usually named as ν_1 (symmetric stretching), ν_2 (symmetric bending), ν_3 (asymmetric stretching), and ν_4 (asymmetric bending). Modes related to pure rotation or translation of the SO_4 units are denoted as R and T, respectively. The translational modes are usually the lowest in frequency, the internal modes are the highest in frequency, and the frequencies of the rotational modes are between those of the translational and internal modes. The modes collected in Table 3 can be organized in three different groups: one group was composed of the first nine modes with a gradual increase of the frequencies from 47 to 264 cm^{-1}. These modes are separated by a phonon gap of nearly 65 cm^{-1} from internal vibrations of SO_4 tetrahedra in their symmetric and asymmetric bending. At high frequency, there are four modes corresponding to symmetric and asymmetric stretching of the SO_4 units. This third group is separated from the second one by a phonon gap of 285 cm^{-1}, according to the experimental spectrum[12]

Table 3. Calculated Phonon Frequencies (cm^{-1}) and Pressure Coefficients (cm^{-1}/GPa) for Anhydrite at Ambient Pressure, Compared to Experimental Values

mode	$\omega(0)$ (cm^{-1})	Ma et al.[12]	$d\omega/dP$	$d\omega/dP$[12]
$T(B_{1g})$	47.4		−1.37	
$T(A_g)$	127.9	123	0.71	
$T(B_{1g})$	134.1	131	−0.34	
$R(B_{3g})$	150.2	168	2.84	
$R(B_{2g})$	158.1		0.07	
$R+T(B_{2g})$	177.1		2.33	
$R+T(B_{1g})$	224.7		7.31	
$T(A_g)$	246.2	235	3.94	
$T(B_{2g})$	264.1		6.95	
$\nu_2(B_{3g})$	329.2	416	−0.67	0.038
$\nu_2(A_g)$	443.5	498	1.81	2.171
$\nu_4(B_{1g})$	516.2	608	0.78	0.950
$\nu_4(B_{2g})$	539.3	626	2.20	1.365
$\nu_4(A_g)$	606.1	674	2.32	1.635
$\nu_1(A_g)$	891.9	1016	4.30	2.722
$\nu_3(B_{1g})$	994.3	1128	4.06	3.226
$\nu_3(A_g)$	1025.1	1159	4.18	3.780
ν_3 (B_{2g})	1042.4	1111	3.90	3.888

dominated by a strong A_g band at 1016 cm^{-1} due to the mode derived from the symmetric stretching vibration (ν_1) of the SO_4 tetrahedra. The phonon frequencies calculated for the anhydrite structure agree reasonably well with those reported in the literature.[12,40] Note that the experiments only report the pressure evolution for the high-frequency modes. Thus, our calculations could be used as a guide for future experiments. In particular, we found several distinctive features for the phonon evolution in anhydrite upon compression. First, the two modes more affected by the pressure are the B_{1g} and B_{2g} modes with frequencies 224.7 and 264.1 cm^{-1}, respectively, associated with a Ca−O stretching. In addition, it can be seen that the anhydrite structure presents three soft modes (at 47, 134, and 329 cm^{-1}) characterized by a decrease of the vibrational frequency with pressure. Softening of the vibrational modes is commonly related to a displacive phase transition. These modes have symmetry B_{1g} and B_{3g} and are associated with a bending between the O−Ca−O units. This feature is typical of scheelite-type structure oxides,[41] suggesting that at higher pressure orthorhombic phases should undergo a transition involving a strong coupling between a zone-center optical mode and a strain, in this case of B_{1g} or B_{3g} symmetry.

In Table 4, the Raman-active modes and their pressure dependences for monazite, barite, and scheelite are presented, at the pressure transition. Monazite displays 36 Raman-active modes at the Γ point, $18A_g + 18B_g$, and all observed modes increase in the frequency with compression. The internal vibrations of the SO_4 tetrahedron cover the frequency range from 400 to 1250 cm^{-1}, with a gap between 727 and 930 cm^{-1}. There are no experimental data to compare with our calculations. However, the calculated evolution of modes is qualitatively similar to that measured in monazite-type $CeVO_4$ and $CePO_4$.[36,42] The absence of soft modes supports the stability of monazite-type $CaSO_4$. We hope our results will trigger new experiments to test our conclusions.

Raman-active modes of the barite-type phase lead to 36 zone-center Raman-active modes: $\Gamma = 11A_g + 7B_{1g} + 7B_{2g} + 11B_{3g}$. The calculated sequence of modes resembles very much that of barite-type oxides. In our case, calculations show that

dx.doi.org/10.1021/ic202056b | Inorg. Chem. 2012, 51, 1751−1759

Table 4. Calculated Phonon Frequencies (cm^{-1}) and Pressure Coefficients (cm^{-1}/GPa) for Monazite at ~5 GPa and Barite and Scheelite at ~8 GPa

monazite			barite			scheelite		
mode	$\omega(0)$	$d\omega/dP$	mode	$\omega(0)$	$d\omega/dP$	mode	$\omega(0)$	$d\omega/dP$
$\nu(A_g)$	8.85	0.63	$\nu(B_{1g})$	60.70	10.37	$T(E_g)$	158.63	1.07
$\nu(B_g)$	29.08	0.41	$\nu(B_{2g})$	85.30	2.07	$T(E_g)$	214.98	4.17
$\nu(A_g)$	49.49	1.48	$\nu(A_g)$	139.12	5.97	$T(B_g)$	201.97	4.73
$\nu(B_g)$	67.75	0.50	$\nu(A_g)$	147.80	2.95	$R(A_g)$	216.78	8.01
$\nu(A_g)$	86.03	1.10	$\nu(B_{3g})$	165.36	2.37	$T(B_g)$	272.79	7.14
$\nu(B_g)$	107.33	0.68	$\nu(B_{1g})$	175.11	6.70	$R(E_g)$	317.67	5.62
$\nu(A_g)$	128.80	1.74	$\nu(B_{2g})$	181.81	3.37	$\nu_2(A_g)$	407.94	4.31
$\nu(A_g)$	150.08	0.25	$\nu(B_{2g})$	185.51	3.28	$\nu_2(B_g)$	431.78	3.21
$\nu(B_g)$	156.70	0.54	$\nu(B_{1g})$	202.92	2.37	$\nu_4(E_g)$	556.71	3.89
$\nu(B_g)$	211.95	0.22	$\nu(B_{3g})$	210.23	5.53	$\nu_4(B_g)$	568.47	4.55
$\nu(B_g)$	249.38	0.72	$\nu(A_g)$	209.84	6.39	$\nu_1(A_g)$	908.55	9.15
$\nu(A_g)$	262.36	2.86	$\nu(B_{2g})$	235.14	2.69	$\nu_3(E_g)$	997.60	9.62
$\nu(A_g)$	272.94	0.80	$\nu(B_{3g})$	241.45	7.57	$\nu_5(B_g)$	1053.97	10.34
$\nu(B_g)$	282.94	0.82	$\nu(A_g)$	254.06	8.31			
$\nu(B_g)$	332.42	0.60	$\nu(B_{3g})$	255.60	9.13			
$\nu(A_g)$	343.27	1.43	$\nu(B_{1g})$	270.51	3.59			
$\nu(A_g)$	408.63	0.28	$\nu(A_g)$	295.39	10.60			
$\nu(B_g)$	418.82	0.87	$\nu(B_{3g})$	339.66	6.08			
$\nu(B_g)$	476.83	1.63	$\nu(A_g)$	413.06	3.61			
$\nu(A_g)$	497.76	1.61	$\nu(B_{3g})$	418.85	4.13			
$\nu(B_g)$	514.45	0.93	$\nu(B_{1g})$	443.24	4.13			
$\nu(A_g)$	524.47	0.42	$\nu(B_{2g})$	453.67	3.88			
$\nu(B_g)$	560.99	2.02	$\nu(A_g)$	567.66	2.71			
$\nu(A_g)$	555.06	0.12	$\nu(B_{3g})$	578.85	3.08			
$\nu(B_g)$	636.10	3.08	$\nu(B_{1g})$	579.31	1.80			
$\nu(A_g)$	640.68	1.32	$\nu(B_{2g})$	580.16	1.94			
$\nu(A_g)$	707.92	8.25	$\nu(A_g)$	604.27	3.45			
$\nu(B_g)$	726.72	3.55	$\nu(B_{3g})$	633.42	3.15			
$\nu(A_g)$	930.34	1.78	$\nu(A_g)$	954.25	5.87			
$\nu(B_g)$	934.24	2.38	$\nu(B_{3g})$	972.03	5.02			
$\nu(A_g)$	1003.59	0.35	$\nu(B_{2g})$	1083.55	5.85			
$\nu(B_g)$	1025.55	0.55	$\nu(B_{1g})$	1086.46	5.49			
$\nu(A_g)$	1069.33	0.78	$\nu(A_g)$	1085.23	4.37			
$\nu(B_g)$	1106.11	1.47	$\nu(B_{3g})$	1133.73	5.45			
$\nu(A_g)$	1194.20	2.84	$\nu(A_g)$	1137.21	5.61			
$\nu(B_g)$	1238.27	4.16	$\nu(B_{3g})$	1181.45	5.37			

Table 5. IR-Active Modes, Their Pressure Shifts, and Grüneisen Parameters for Anhydrite at Ambient Pressure, Compared to Experimental Values

anhydrite				Bradbury and Williams[13]		
mode	$\omega(0)$	$d\omega/dP$	γ	mode	$\omega(0)$	$d\omega/dP$
$T(B_{2u})$	155.51	0.17	0.17			
$R+T(B_{1u})$	183.80	2.36	2.36			
$R+T(B_{2u})$	231.61	10.67	10.67			
$T(B_{3u})$	241.32	5.83	5.83			
$T(B_{1u})$	275.13	7.04	7.04			
$\nu_4(B_{3u})$	458.05	2.36	2.36			
$\nu_4(B_{1u})$	488.72	0.93	0.93	$\nu_3(B_{1u}+B_{2u}+B_{3u})$	593	0.43
$\nu_4(B_{2u})$	513.77	0.99	0.99		610	0.12
$\nu_4(B_{3u})$	599.69	2.21	2.21		674	1.98
$\nu_1(B_{2u})$	886.01	4.57	4.57	$\nu_1(B_{2u})$	1019[a]	
$\nu_3(B_{1u})$	981.19	5.01	5.01			
$\nu_3(B_{2u})$	1007.55	3.96	3.96	$\nu_4(B_{1u}+B_{2u}+B_{3u})$	1104	4.39
$\nu_3(B_{3u})$	1044.24	5.13	5.13		1189	0.79

[a]At 2.1 GPa.

dx.doi.org/10.1021/ic202056b | Inorg. Chem. 2012, 51, 1751−1759

Table 6. IR-Active Modes, Their Pressure Shifts, and Grüneisen Parameters for Monazite at 5 GPa, Compared to Experimental Values at 8.5 GPa

monazite				Bradbury and Williams[13]			
mode	$\omega(0)$	$d\omega/dP$	γ	mode	$\omega(0)$	$d\omega/dP$	γ
$R(A_u)$	58.05	0.15	3.00				
$R+T(B_u)$	69.59	0.69	6.25				
$R(B_u)$	88.44	0.52	2.10				
$R+T(A_u)$	110.88	0.74	1.90				
$T(B_u)$	122.54	0.85	1.81				
$T(B_u)$	180.63	6.79	10.20				
$T(A_u)$	216.96	4.17	4.16				
$R+T(A_u)$	266.66	0.65	0.44				
$R(B_u)$	317.54	1.28	0.71				
$T(B_u)$	320.56	0.73	0.40				
$R(A_u)$	338.06	0.33	0.17				
$R(A_u)$	413.11	0.91	0.37				
$R(B_u)$	421.40	0.48	0.19				
$R(B_u)$	453.48	0.96	0.35				
$R+T(A_u)$	462.89	2.06	0.75				
$R+T(A_u)$	519.67	1.89	0.60				
$R+T(B_u)$	539.09	0.24	0.07				
$\nu_4(A_u)$	553.17	1.04	0.31				
$\nu_4(A_u)$	571.79	0.44	0.12				
$\nu_4(B_u)$	591.52	3.00	0.83	$\nu_4(3A_u+3B_u)$	592	0.99	0.25
$\nu_4(B_u)$	611.35	3.19	0.85		621	1.79	0.43
$\nu_4(B_u)$	681.51	0.82	0.19		639	1.87	0.44
$\nu_4(A_u)$	698.62	2.47	0.57		672	0.89	0.20
$\nu_4(B_u)$	742.31	6.83	1.51				
$\nu_4(A_u)$	753.54	2.07	0.44				
$\nu_1(A_u)$	965.81	2.51	0.41				
$\nu_1(B_u)$	984.92	1.90	0.30	$\nu_1(A_u+B_u)$	1030	4.33	0.63
$\nu_3(B_u)$	1049.41	1.87	0.28				
$\nu_3(A_u)$	1073.42	5.16	0.76				
$\nu_3(A_u)$	1108.32	1.51	0.21	$\nu_3(3A_u+3B_u)$	1109	4.44	0.60
$\nu_3(B_u)$	1156.92	1.80	0.24		1201	3.94	0.49
$\nu_3(B_u)$	1247.24	0.88	0.11		1268	3.98	0.47
$\nu_3(A_u)$	1275.21	2.79	0.34				

lattice modes for frequencies smaller than 350 cm^{-1} are basically ascribed to the motion of the Ca cation and tetrahedral SO_4 units. The internal vibrations of the SO_4 tetrahedron spanned the frequency range from 400 to 1200 cm^{-1} but with a gap between 633 and 954 cm^{-1}. The modes located between 954 and 1181 cm^{-1} can be associated with the ν_1 and ν_3 bands of barite.[43] For this structure, the modes with larger pressure coefficients are located below 350 cm^{-1}. $CaSO_4$ with scheelite structure has 13 Raman-active modes corresponding to the following decomposition at the Γ point: $\Gamma = 3A_g + 5B_g + 5E_g$. This structure also presents two phonon gaps, one of them at 90 cm^{-1} from rotational and translational modes to the internal bending modes of the SO_4 units and the second gap between the frequencies of the internal stretching modes and the rest of the modes (from 568 to 908 cm^{-1}). This is typical of ABO_4 oxides and is basically related to the fact that the ν_1 and ν_3 modes involve movements of the less compressible bonds of the crystal (S−O). The pressure dependence of the different modes of the barite- and scheelite-type phases is also reported in Table 4. The obtained behavior is comparable to that of isomorphic oxides.

Finally, in Tables 5 and 6, the IR-active modes and their pressure dependences for anhydrite and monazite structures are presented, respectively, compared to experimental values. As expected, all modes increase in the frequency with pressure and vibrations involving calcium translations are likely to have larger Grüneisen parameters for both anhydrite and monazite phases. Anhydrite has 13 vibrations that are IR-active corresponding to $\Gamma = 4B_{1u} + 5B_{2u} + 4B_{3u}$, and for monazite, the irreducible representation of the optic vibrations generates 33 IR-active modes, $\Gamma = 17A_u + 16B_u$. The number of IR-active modes arising from the normal vibrations of the sulfate tetrahedra are doubled in the high-pressure phase, in accordance with Bradbury and Williams.[13] However, we find one and two asymmetric bending vibrations more than they reported for anhydrite and monazite, respectively. In addition, the reported assignation of modes for the asymmetric stretching (ν_3) and asymmetric bending (ν_4) vibrations in anhydrite seem to be intercambiated because, according to vibrational expectations, stretching modes appear usually at higher frequency values than bending modes.

4. CONCLUSION

On the basis of quantum-chemical simulations, we provide the systematic investigation of the structural properties of the possible calcium sulfate $CaSO_4$ polymorphs. The geometry and vibrational properties have been characterized for the different bulk phases, and their response to hydrostatic pressure has been

dx.doi.org/10.1021/ic202056b | Inorg. Chem. 2012, 51, 1751−1759

reported. The main results can be summarized as follows: (i) We have characterized anhydrite and four structures of $CaSO_4$ at high *P*: the monazite, barite, and scheelite types and a possible orthorhombic $P2_12_12_1$. (ii) We do not have evidence for the existence of the barite distorted-$AgMnO_4$ variant. (iii) Although the coordination of the S atom does not change along with the pressure, the tilting movement of the $[SO_4]$ tetrahedra led to a change in the environment of the Ca atoms along the phase transitions from 8 in anhydrite to 9 in monazite and 12 in barite, involving an enlargement of the Ca−O bonds in order to accommodate the new O atoms surrounding the Ca atoms. The pressure evolution of the unit-cell parameters of $CaSO_4$ has been analyzed, obtaining an anisotropic compression of the anhydrite and scheelite forms. (iv) The values of the phonon frequencies, Raman and IR, as well as their pressure dependence for the different phases have been reported and compared to different experimental data, with the different modes being assigned based upon our calculations and assuming that in the different structures the SO_4 tetrahedra are nearly isolated units.

We hope that this comprehensive study serves as a guideline for the interpretation of various experiments involving different phases of the $CaSO_4$ system, and on related complex oxides, as well as for the interpretation of the presently reported results. We expect that the results here reported will trigger new theoretical and experimental studies.

AUTHOR INFORMATION

Corresponding Author

*E-mail: lgracia@qfa.uji.es.

Notes

‡MALTA Consolider Team.

ACKNOWLEDGMENTS

This work was supported by the Spanish MALTA-Consolider Ingenio 2010 Program (Project CSD2007-00045), Bancaixa Foundation (P11B2009-08), Spanish MICINN (Grants CTQ2009-14541-C02 and MAT2010-21270-C04-01), and Generalitat Valenciana (Project Prometeo/2009/053). The authors also acknowledge the Servei Informatica, Universitat Jaume I, for a generous allotment of computer time.

REFERENCES

(1) Nyman, H.; Hyde, B. G.; Andersson, S. *Acta Crystallogr., Sect. B* **1984**, *40*, 441−447.

(2) Errandonea, D.; Manjon, F. J. *Prog. Mater. Sci.* **2008**, *53*, 711−773.

(3) Errandonea, D.; Kumar, R.; Lopez-Solano, J.; Rodriguez-Hernandez, P.; Munoz, A.; Rabie, M. G.; Puche, R. S. *Phys. Rev. B* **2011**, *83*, 134109.

(4) Errandonea, D.; Santamaria-Perez, D.; Achary, S. N.; Tyagi, A. K.; Gall, P.; Gougeon, P. *J. Appl. Phys.* **2011**, *109*, 043510.

(5) Baran, E. J. *J. Mater. Sci.* **1998**, *33*, 2479−2497.

(6) Kahn, J. S. *Science* **1975**, *189*, 454−455.

(7) Chen, C. C.; Liu, L. G.; Lin, C. C.; Yang, Y. J. *J. Phys. Chem. Solids* **2001**, *62*, 1293−1298.

(8) Borg, I. Y.; Smith, D. K. *Contrib. Mineral. Petrol.* **1975**, *50*, 127−133.

(9) Crichton, W. A.; Parise, J. B.; Antao, S. M.; Grzechnik, A. *Am. Mineral.* **2005**, *90*, 22−27.

(10) Lacomba-Perales, R.; Errandonea, D.; Meng, Y.; Bettinelli, M. *Phys. Rev. B* **2010**, *81*, 064113.

(11) Pistorius, C. W.; Boeyens, J. C. A.; Clark, J. B. *High Temp.-High Press.* **1969**, *1*, 41−52.

(12) Ma, Y. M.; Zhou, Q.; He, Z.; Li, F. F.; Yang, K. F.; Cui, Q. L.; Zou, G. T. *J. Phys.: Condens. Matter* **2007**, 19.

(13) Bradbury, S. E.; Williams, Q. *J. Phys. Chem. Solids* **2009**, *70*, 134−141.

(14) Martin, R. M. *Electronic Structure: Basic Theory and Practical Methods*; Cambridge University Press: Cambridge, U.K., 2005.

(15) Santamaría-Pérez.; Gracia, L.; Garbarino, G.; Beltrán, A.; Chuliá-Jordán, R.; Gomis, O.; Errandonea, D.; Ferrer-Roca, C.; Martínez-García, D.; Segura, A. *Phys. Rev. B* **2011**, *84*, 054102.

(16) Parise, J. B.; Antao, S. M.; Martin, C. D.; Crichton, W. *Powder Diffr.* **2005**, *20*, 80−86.

(17) Clavier, N.; Podor, R.; Dacheux, N. *J. Eur. Ceram. Soc.* **2011**, *31*, 941−976.

(18) Dovesi, R.; Saunders, V. R.; Roetti, C.; Orlando, R.; Zicovich-Wilson, C. M.; Pascale, F.; Civalleri, B.; Doll, K.; Harrison, N. M.; Bush, I. J.; D'Arco, P.; Llunell, M. *CRYSTAL09 Program*; Torino, Italy, 2010. http://www.crystal.unito.it/Manuals/crystal09.pdf.

(19) Becke, A. D. *J. Chem. Phys.* **1993**, *98*, 5648−5652.

(20) Lee, C. T.; Yang, W. T.; Parr, R. G. *Phys. Rev. B* **1988**, *37*, 785−789.

(21) Hu, C.-H.; Chong, D. P. *Density Functional Applications, in Encyclopedia of Computational Chemistry*; Wiley: Chichester, U.K., 1998; Vol. *1*.

(22) Gracia, L.; Beltrán, A.; Errandonea, D. *Phys. Rev. B* **2009**, *80*, 094105.

(23) Gracia, L.; Beltrán, A.; Andrés, J. *J. Phys. Chem. C* **2011**, *115*, 7740−7746.

(24) Blanco, M. A.; Francisco, E.; Luaña, V. *THEOCHEM* **2004**, *158*, 57.

(25) Lopez-Solano, J.; Rodriguez-Hernandez, P.; Munoz, A.; Gomis, O.; Santamaria-Perez, D.; Errandonea, D.; Manjon, F. J.; Kumar, R. S.; Stavrou, E.; Raptis, C. *Phys. Rev. B* **2010**, *81*, 144126.

(26) Zhang, F. X.; Wang, J. W.; Lang, M.; Zhang, J. M.; Ewing, R. C.; Boatner, L. A. *Phys. Rev. B* **2009**, *80*, 184114.

(27) Kirfel, A.; Will, G. *Acta Crystallogr., Sect. B* **1980**, *36*, 2881−2890.

(28) Vegas, A. *Crystallogr. Rev.* **2000**, *7*, 189.

(29) Boonstra, E. G. *Acta Crystallogr., Sect. B* **1968**, *B 24*, 1053−1062.

(30) Errandonea, D.; Kumar, R. S.; Gracia, L.; Beltrán, A.; Achary, S. N.; Tyagi, A. K. *Phys. Rev. B* **2009**, *80*, 094101.

(31) Errandonea, D.; Gracia, L.; Beltrán, A.; Vegas, A.; Meng, Y. *Phys. Rev. B* **2011**, *84*, 064103.

(32) Stephens, D. R. *Geophys. Res.* **1964**, *69*, 2967−&.

(33) Errandonea, D.; Schwager, B.; Boehler, R.; Ross, M. *Phys. Rev. B* **2002**, 65.

(34) Errandonea, D.; Meng, Y.; Somayazulu, M.; Hausermann, D. *Phys. B (Amsterdam, Neth.)* **2005**, *355*, 116−125.

(35) Lacomba-Perales, R.; Martinez-Garcia, D.; Errandonea, D.; Le Godec, Y.; Philippe, J.; Le Marchand, G.; Chervin, J. C.; Polian, A.; Munoz, A.; Lopez-Solano, J. *Phys. Rev. B* **2010**, *81*, 144117.

(36) Panchal, V.; Manjon, F. J.; Errandonea, D.; Rodriguez-Hernandez, P.; Lopez-Solano, J.; Munoz, A.; Achary, S. N.; Tyagi, A. K. *Phys. Rev. B* **2011**, *83*, 064111.

(37) Stubican, V. S.; Roy, R. *J. Appl. Phys.* **1963**, *34*, 1888−&.

(38) Bedlivy, D.; Mereiter, K. *Acta Crystallogr., Sect. B* **1982**, *38*, 1559−1561.

(39) Macey, B. J. The crystal chemistry of MTO4 compounds with the zircon, scheelite and monazite structure types. Master Thesis, 1995; Virginia Tech, Blacksburg, 69 pp.

(40) Lishi, K. *Phys. Chem. Mineral.* **1979**, *4*, 341.

(41) Errandonea, D.; Manjón, F. J. *Mater. Res. Bull.* **2009**, *44*, 807−811.

(42) Huang, T.; Lee, J. S.; Kung, J.; Lin, C. M. *Solid State Commun.* **2010**, *150*, 1845−1850.

(43) Chen, Y. H.; Huang, E.; Yu, S. C. *Solid State Commun.* **2009**, *149*, 2050−2052.